[PROC. OF JSCE No. 424/III-14 (Geotechnical Eng.) December 1990]

ANALYSIS OF PERMANENT GROUND DEFORMATION DUE TO LIQUEFACTION WITH DISTINCT ELEMENT MODEL

By Shunichi IGARASHI and Kimiro MEGURO***

The permanent displacement of a slope in Noshiro city during the 1983 Nihonkai-Chubu earthquake is simulated by Distinct Element Analysis. The slope of 2.6 degrees average inclination and 200 m length is modeled as 3 180 element Distinct Element Model (DEM). A FEM model of 611 quadrilateral elements is utilized to verify the DEM model in the small displacement range. In quasi-static analysis using lateral seismic coefficients of 0.1~0.3, both FEM and DEM models are found to give similar failure surface and critical acceleration, i.e., threshold acceleration for initiating failure. Some subsurface layers are supposed to have been liquefied during the earthquake ground motion. In the model, both the stiffness and shearing resistance of these layers are reduced to account for their volumetric change and liquefaction. The movement of the slope due to subsurface soil liquefaction is simulated realistically with the DEM model including vertical crack and settlement at the top of the slope and lateral sliding of the surface layers. From parametric studies, volumetric change of the liquefied layer is found to be the most influential factor to induce deformation of the slope.

Keywords: distinct element analysis, permanent displacement, ground motion, simulation, distinct element method (DEM)

1. INTRODUCTION

Since the 1964 Niigata earthquake, liquefaction has been identified as a major cause of structural damage. Hamada, Yasuda, Isoyama and Emoto [1986] by using aerial photographs, identified that there had been a large permanent ground displacement in Niigata city during the 1964 earthquake. They concluded that the movement of ground was caused by the liquefaction of layers underneath. They pointed out various evidences of this astonishing phenomenon including breaking of piles of Niigata TV station found only after an excavation for the reconstruction project in 1985.

Analysis of the permanent ground displacement due to liquefaction has following difficulties:

1) The permanent displacement takes place in a large area with its magnitude of several meters.

2) The permanent displacement in ground can include vertical cracks, movement inside of the liquefied layers.

3) The shearing resistance in soil layers may change drastically during shaking. Associated movement can alter the configuration of the soil strata in a large scale.

The discontinuity and nonstationarity inherent in the soil-structure interaction problem is conspicuous in this phenomenon. Conventional method of analysis represented by the FEM idealization can only simulate the permanent displacement as is averaged over some range of modeling. The difference between the FEM model and actual configuration will be considerably large during and after the permanent displacement.

The sliding block model proposed by Newmark (1965) can simulate the movement of the ground along with the discontinuity between the liquefied layer and sound layers. However it cannot capture the change

* Member of JSCE, Dr. Eng., Taisei Corp. (Nishishinjuku 1-25-1 Shinjuku-ku, Tokyo 163, Japan)
** Member of JSCE, M. Eng., Graduate Student, Department of Civil Engineering, University of Tokyo (Yayoi 1-1-1 Bunkyo-ku, Tokyo 113, Japan)

in the configuration and associated internal resistance that alters the critical acceleration.

In 1965 Mogami proposed an approach to the idealization of mechanics of soil with granular elements. Cundall (1971) developed a discrete numerical model to simulate the behavior of granular assemblies (Distinct Element Method). This model idealizes target structure as an assembly of elastic elements and focuses only on the contact forces between neighboring elements. This method of discretization allows us to simulate the configuration change in the structure realistically with a collection of granular elements. The sliding block model can be regarded as the simplest version of the Distinct Element Method that uses only one element along with a boundary condition. A new method of analysis can be constructed using the Distinct Element Model instead of the simple mass-on-rough-plane model in the procedure of the sliding block analysis. This method will be applied to simulate the permanent ground displacement in Noshiro city during the 1983 Nihonkai-Chubu earthquake. The result will be compared with the actual behavior of the ground measured by Hamada *et al.* (1986).

2. PROCEDURE OF ANALYSIS

(1) Distinct element analysis

The elements of sliding block analysis include :

1) Pseudo-static analysis to compute critical acceleration of the structure.

2) Dynamic response analysis to calculate the time history of the effective acceleration that is averaged over the potential sliding portion of the structure.

3) Dynamic response analysis of the mass-on-rough-plane model due to the effective acceleration to obtain the residual displacement of the mass that simulates the actual mean permanent displacement of the sliding portion of the structure. The sliding block analysis is actually an assembly of these pseudo-static and dynamic analysis. The consistency of the total analysis is ensured only in terms of the forces and accelerations that are passed through member analyses.

The Distinct Element Analysis of permanent ground displacement will be constructed replacing the mass-on-rough-plane model with the Distinct Element Model in the above mentioned flow. Fig. 1 illustrates the elements and flow of this analysis. Firstly, a global FEM elastic-plastic model is constructed to compute the critical acceleration of the ground by pseudo-static analysis. The critical acceleration is the one that brings a limit equilibrium into the structure. This can be obtained by increasing seismic

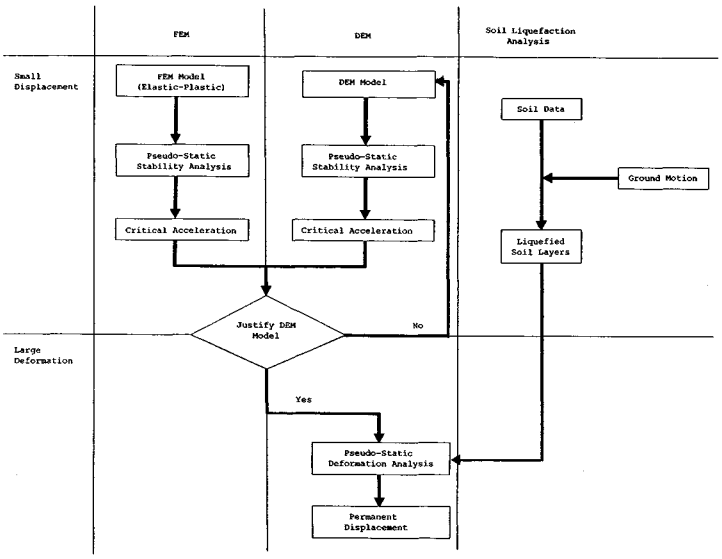

Fig. 1 Flow of Distinct Element Analysis of permanent ground displacement.

coefficients little by little in the global FEM model (Igarashi and Hakuno, 1987). In this study, the vertical seismic coefficient is set to zero considering the consistency with the 1-D soil liquefaction analysis used to identify the liquefied layer.

Secondly, the DEM model is constructed so as to possess the same critical acceleration with the actual ground that was computed using the global FEM model. This critical acceleration is the one in the ordinary state without soil liquefaction.

Thirdly, permanent deformation of the ground is calculated by pseudo-static analysis of a DEM model. The effect of liquefaction is included by reducing both shearing resistance and stiffness of the elements in the soil layers that are identified as 'liquefied' in the 1-D soil liquefaction analysis.

(2) Distinct element idealization of soil

Distinct Element Method idealizes soil as an assembly of circular (distinct) elements as shown by dashed lines in Fig. 2(a). The size of every element is set to 0.75 m in this analysis. Distinct element does not represent a particle of soil but a lump of soil consisting of particles, pore water and voids.

Fig. 2(b) shows three elements. Between adjoining elements, contact forces (shear and compression) and 'pore forces' (shear, compression and tension) are considered. The element boundary is the circumference where it is judged for contact with other elements. When pore boundaries of the adjoining elements are overlapped (Fig. 2(b)), the 'pore force' is exerted on them. The element and pore springs depicted in Figs. 2(c) and 2(d) show different forces mechanically.

The equations of motion of an element with the mass m and the moment of inertia I are

$$m\ddot{u}+C\dot{u}+F=0 \quad (1)$$

$$I\ddot{\phi}+D\dot{\phi}+M=0 \quad (2)$$

where C and D are the viscous damping coefficients and u and ϕ the translational and rotational displacements respectively. The resultant of the external forces F consists of

$$F=\sum f_e+\sum f_p+(a+g)m \quad (3)$$

with a and g being the external and gravity accelerations respectively and $\sum f_e$ represents contact forces from all the elements in touch with this element. The pore force is denoted by f_p and illustrated in Fig. 2 (b). This force acts so as to maintain the initial distance where the pore material force originally appeared.

The total moment of the element in Eq. (2) is

$$M=\sum M_e+\sum M_p \quad (4)$$

where $\sum M_e$ is the sum of all the moments acting on the element by all the contacting elements, and $\sum M_p$ that by pore material surrounding it.

The configuration of the total system u an ϕ can be computed by integrating Eqs. (1) and (2) with

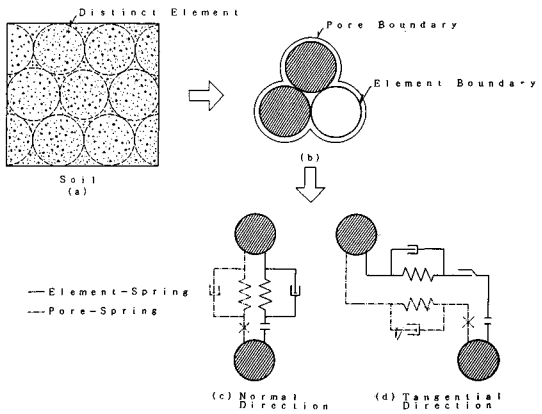

Fig. 2 Distinct Element Idealization of Soil.

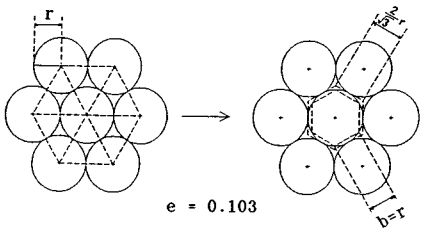

Fig. 3 Relationship between particle disposition and contact length.

respect to time. The external forces F and M in these equations are function of incremental relative displacements namely relative velocity and relative displacement between elements. The numerical integration method should be carefully selected. The most primitive yet the best choice in terms of stability and accuracy is to take the smallest possible incremental time. In this study an explicit numerical integration with the trapezoidal rule is employed.

The parameters of the DEM model are determined as follows (Meguro *et al.*, 1988).

The mass of an element, m, is determined so as to include that of soil and pore water in the soil structure.

$$m=\pi r^2(1+e)\rho \quad (5)$$

where ρ is the density of the soil and e is the void ratio of the model. In this analysis, circular elements of radius $r=0.75$ m are arranged so that their centers consist equilateral triangles (Fig. 3). The void ratio of this arrangement is

$$e=0.103 \quad (6)$$

Element spring constants represent contact forces between elements. They will be computed from Young's modulus, E, Poisson's ratio, ν, and density of the soil, ρ. Firstly, the primary wave velocity V_p and the secondary wave velocity V_s are computed.

$$V_p=\sqrt{(1-\nu)E/(\rho(1-2\nu)(1+\nu))} \quad (7)$$

$$V_s=\sqrt{E/(2\rho(1+\nu))} \quad (8)$$

Spring constant K_n for contact force in the direction of element centers (see Fig. 2) are determined from the P wave velocity.

$$K_n=\pi\rho V_p^2/4 \quad (9)$$

The shearing spring constant is

$$K_s=\pi\rho V_s^2/4 \quad (10)$$

These spring constants are allocated to element spring K_{en}, K_{es} and pore spring K_{pn}, K_{ps} so as to have for normal springs

$$\frac{1}{K_n}=\frac{1}{K_{en}}+\frac{1}{K_{pn}} \quad (11)$$

and for shearing springs

$$\frac{1}{K_s}=\frac{1}{K_{es}}+\frac{1}{K_{ps}} \quad (12)$$

We assume a linear relationship between pore springs K_{pn} and K_{ps} and element springs K_{en} and K_{es} as follows:

$$K_{pn}=t_nK_{en},\quad K_{ps}=t_sK_{es} \quad (13)$$

Iwashita (1988) suggested $t_n=t_s=0.1$ for sandy soil. This value is used in this analysis.

The pore spring is established when ever the central distance, $[D_{ij}]$, between the two elements, i and j, is smaller than α times the sum of the radii of the two elements, (r_i+r_j):

$$[D_{ij}]\leqq\alpha(r_i+r_j) \quad (14)$$

α : see Table 2

Two states of the pore-spring are incorporated in the DEM:

State 1 : The pore spring is normal. In this state it resists not only compression but tension and shearing when external compressive or tensile forces act on it.

State 2 : Crack is produced in the pore spring. It has no tensile resistance. It resists compressive and shearing deformation only while compressive force acts between the elements.

The fracture of the pore-spring is produced by following two conditions.

1) In the normal direction : The pore-spring loses tension resistance when the distance of the two elements exceeds β times the initial length of the pore-spring, $L_{ij}=[D_{ij}]_0$.

$$D_{ij}\geqq\beta L_{ij} \quad (15)$$

β : see Table 2

where L_{ij} is the central distance of the two elements where the pore spring appears.

2) In the tangential direction : The pore-spring will break when the tangential force F_t exceeds the Mohr-Coulomb's limit

$$F_t \leqq F_n \tan\theta + bC \quad \cdots\cdots (16)$$

where F_n is the normal force acting on the contact surface, C and θ being the cohesion and the angle of internal friction respectively. The multiplier b is a constant to produce critical shear force from cohesive stress. Its choice depends on the arrangement of elements. From Fig. 3, the friction contact length b is assumed to be

$$b = r \quad \cdots\cdots (17)$$

3. MODELS OF ANALYSIS

(1) Simulated ground displacement

Hamada *et al.* (1986) reported a result of detailed survey and analysis of the permanent ground displacement in Noshiro city during the 1983 Nihonkai-Chubu earthquake. Fig. 4 illustrates the measured displacements of the southern part of Noshiro City. The S-13 section is selected in this analysis. Fig. 5(a) illustrates the soil condition reported by Hamada *et al.* (1986). The shaded zones were estimated to have liquefied during the earthquake considering the Fl values computed for the peak ground surface acceleration of 250 gal. This value was obtained from an attenuation analysis using the location of the epicentral zone of the earthquake (Fig. 6). Fig. 5(b) illustrates the magnitudes of the estimated displacements from the aerial photographs. The modeling area is selected at the L=200 m zone shown in Fig. 5(a). The average inclination of the ground surface is about 2.6 degrees. A maximum horizontal displacement is estimated about 3 m. The duration of the movement is not recorded, but Hamada *et al.* report that some residents heard strange sound that might have been caused by the ground displacement 60 minutes after the earthquake.

(2) FEM model

The ground is assumed to consist of a total of 10 layers with pertinent parameters listed in Table 1. An FEM model is made to analyze the critical acceleration of the ground without soil liquefaction. Fig. 7

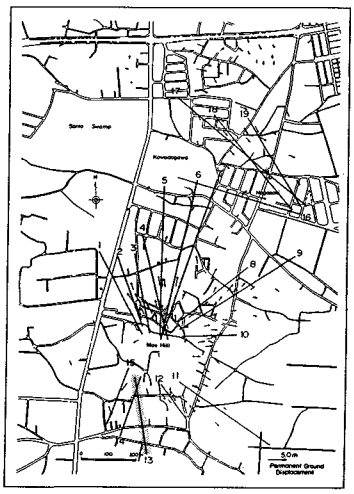

Fig. 4 Permanent ground displacement of the Southern part of Noshiro city during the 1983 Nihonkai-Chubu earthquake (after Hamada *et al.*, 1986).

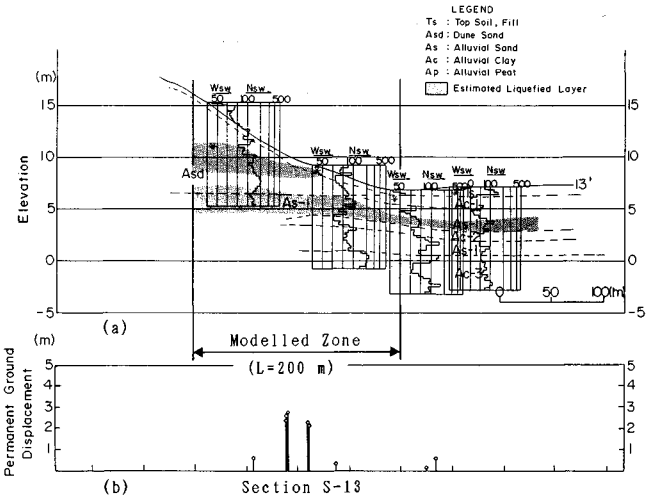

Fig. 5 Boring logs and measured displacement of section S-13 (after Hamada *et al.*, 1986).

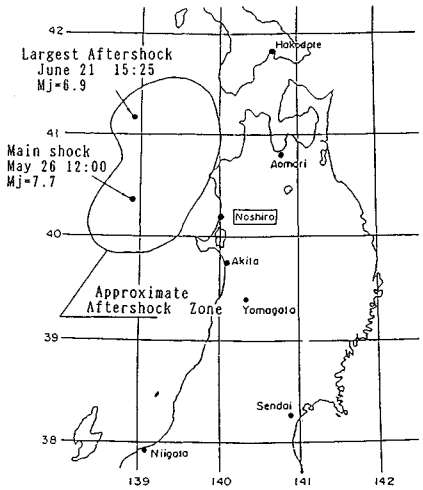

Fig. 6 Noshiro city and epicentral zone of the 1983 Nihonkai-Chubu earthquake.

Table 1 Pertinent Parameters of Soil Strata.

Soil Strata	Young's Mod. (t/m^2)	Poisson's Rat.	Density (Ord.) (t/m^3)	Density (Seismic) (t/m^3)	Cohesion (t/m^2)	Friction Ang. (deg)
① Ts Surface fine sand	1560	0.33	1.80	1.80	0	35.0
② Ac1 Silt	2440	0.45	0.65	1.65	10	0.0
③ Asd Silt/Sand Above W.	2960	0.33	1.80	1.80	0	35.0
④ Asd ditto Below W.	3280	0.33	1.00	2.00	0	35.0
⑤ Asd ditto	3280	0.33	1.00	2.00	0	35.0
⑥ Asl Silt/Sand	5500	0.33	0.80	1.80	0	35.0
⑦ Ac2 ditto	5600	0.45	0.68	1.68	10	0.0
⑧ Asl ditto	5500	0.33	0.80	1.80	0	35.0
⑨ Ac3 Silt	9760	0.45	0.65	1.65	0	35.0
⑩ Base Layer(Fictious)	9760	0.45	0.65	1.65	1000	0.0

Note: Above W. denotes The layer is above the Water table.
Below W. is likewise.

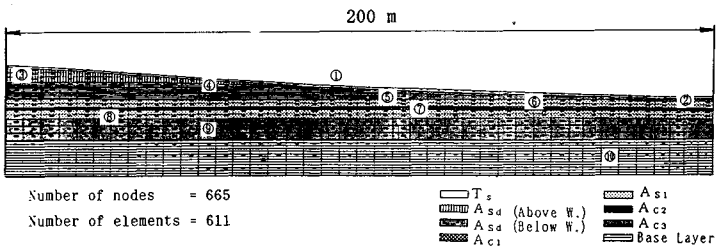

Fig. 7 FEM Model of Noshiro S-13 Section.

illustrates the meshes of the FEM model with 611 4-node quadrilateral plane strain elements. The materials are assumed to be elastic plastic and to follow the Mohr-Coulomb constitutive law with the c and θ parameters as listed in Table 1.

(3) Distinct element model

Fig. 8 shows the DEM model. This model idealizes L=200 m portion of the slope depicted in Fig. 5. Down to 31.5 m below the ground surface is modeled and is divided into 10 layers. It has 3 180 circular elements of 0.75 m radius and 189 boundary elements. The model parameters are listed in Table 2. They are computed from the pertinent soil parameters listed in Table 1 in the procedures illustrated in Sec. 2. (2).

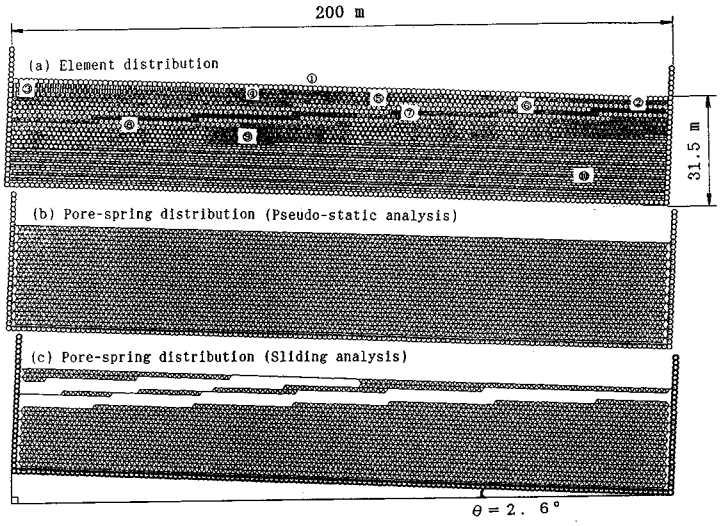

Fig. 8 DEM Model of Noshiro S-13 Section.

Table 2 DEM model parameters.

Layers		① Ts	② Ac1	③ Asd	④ Asd Liquefied				⑤ Asd	⑥ As1 Liquefied				⑦ Ac2	⑧ As1	⑨ Ac3	⑩
					Normal	Case 1	Case 2	Case 3		Normal	Case 1	Case 2	Case 3				
Element Spring (Normal)	Ken (N/m)	2.0 x10⁶	8.0 x10⁶	3.8 x10⁶	4.2 x10⁶	4.2 x10⁵	8.4 x10⁴	4.2 x10⁴	4.2 x10⁶	7.0 x10⁶	7.0 x10⁵	1.4 x10⁵	7.0 x10⁴	1.9 x10⁷	7.0 x10⁶	3.2 x10⁷	3.2 x10⁷
Element Spring (Tangential)	Kes (N/m)	5.1 x10⁵	7.3 x10⁵	9.7 x10⁵	1.1 x10⁶	1.1 x10⁵	2.2 x10⁴	1.1 x10⁴	1.1 x10⁶	1.8 x10⁶	1.8 x10⁵	3.6 x10⁴	1.8 x10⁴	1.7 x10⁶	1.8 x10⁶	3.0 x10⁶	3.0 x10⁶
Damping Coeff. (Normal)	η_n (Nsec/m)	8.4 x10⁴	1.6 x10⁵	1.2 x10⁵	1.3 x10⁵	1.3 x10⁴	1.3 x10⁴	1.3 x10⁴	1.3 x10⁵	1.6 x10⁵	1.6 x10⁴	1.4 x10⁴	1.6 x10⁴	2.5 x10⁵	1.6 x10⁵	3.2 x10⁵	3.2 x10⁵
Damping Coeff. (Tangential)	η_s (Nsec/m)	4.2 x10⁴	4.9 x10⁴	5.9 x10⁴	6.5 x10⁴	6.5 x10³	6.5 x10³	6.5 x10³	6.5 x10⁴	8.0 x10⁴	8.0 x10³	8.0 x10³	8.0 x10³	7.4 x10⁴	8.0 x10⁴	9.7 x10⁴	9.7 x10⁴
Pore Spring (Normal)	Kpn (N/m)	2.0 x10⁵	8.0 x10⁵	3.8 x10⁵	4.2 x10⁵	-	-	-	4.2 x10⁵	7.0 x10⁵	-	-	-	1.9 x10⁶	7.0 x10⁵	3.2 x10⁶	3.2 x10⁶
Pore Spring (Tangential)	Kps (N/m)	5.1 x10⁴	7.3 x10⁴	9.7 x10⁴	1.1 x10⁵	-	-	-	1.1 x10⁵	1.8 x10⁵	-	-	-	1.7 x10⁵	1.8 x10⁵	3.0 x10⁵	3.0 x10⁵
Effective Distance of Pore Springs	α	1.20	1.20	1.20	1.20	-	-	-	1.20	1.20	-	-	-	1.20	1.20	1.20	1.20
Failure Distance of Pore Springs	β	1.02	1.02	1.02	1.02	-	-	-	1.02	1.02	-	-	-	1.02	1.02	1.02	1.02
Element Density	ρ_d (kg/m³)	1998	1832	1998	2220	2220	2220	2220	2220	1998	1998	1998	1998	1865	1998	1832	1832
Effective Element Density	ρ_w (kg/m³)	1998	832	1998	1220	1220	1220	1220	1220	998	998	998	998	865	998	832	832
Friction Coeff.	μ	0.7	0	0.7	0.7	0	0	0	0.7	0.7	0	0	0	0	0.7	0.7	0
Cohesion	C (N)	0	7.1 x10⁴	0	0	0	0	0	0	0	0	0	0	7.1 x10⁴	0	7.1 x10⁴	7.1 x10⁴
Time Step	ΔT (sec)	1.0 x 10⁻³															

Note : Numbers encircled correspond to the layer numbers as indicated in Fig. 8.

4. SIMULATION RESULTS

(1) Critical acceleration and failure mode of the ground by FEM

The critical acceleration of the ground can be defined as the lateral acceleration that brings a limit equilibrium in the system. This can be computed by a pseudo-static analysis with FEM model by increasing seismic coefficient little by little until a total slide occurs in the model. Figs. 9, 10 and 11 show the results of pseudo-static analysis with horizontal seismic coefficients (K_h) of 0.2, 0.25, 0.3, respectively.

In Fig. 9 (K_h=0.2), the sandy silt layers (A_{sd}) beneath the water table reach the Mohr-Coulomb's Failure criteria. In Fig. 9(b) is plotted the local safety factors of this criteria, i.e., the mobilized shear stress over the critical value ($\tau_c = C + N \tan\theta$, with C, N and θ being the cohesion, effective normal stress and internal friction angle, respectively). The displacement in the horizontal direction is almost

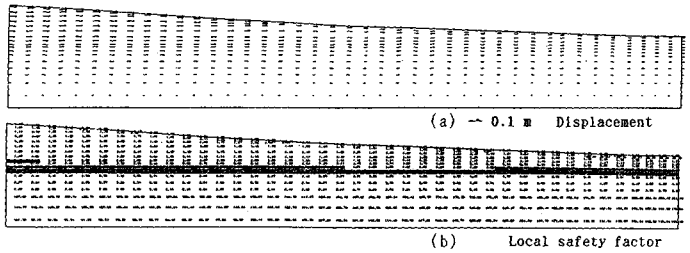

Fig. 9 Result of FEM analysis (K_h=0.2).

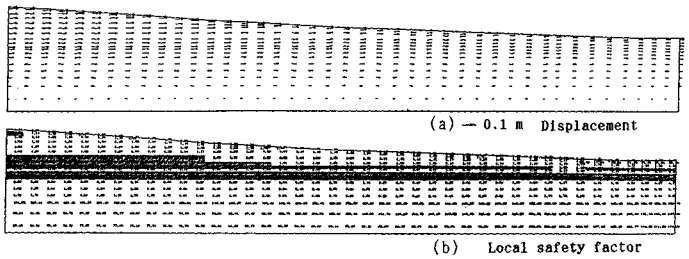

Fig. 10 Result of FEM analysis (K_h=0.25).

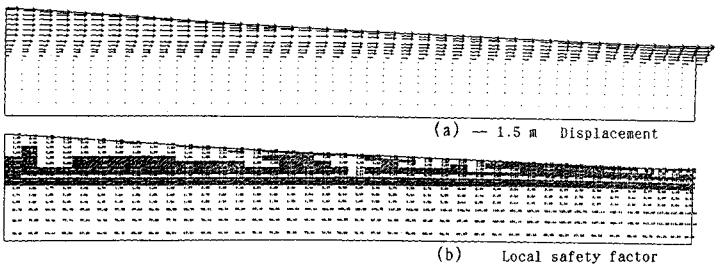

Fig. 11 Result of FEM analysis (K_h=0.3).

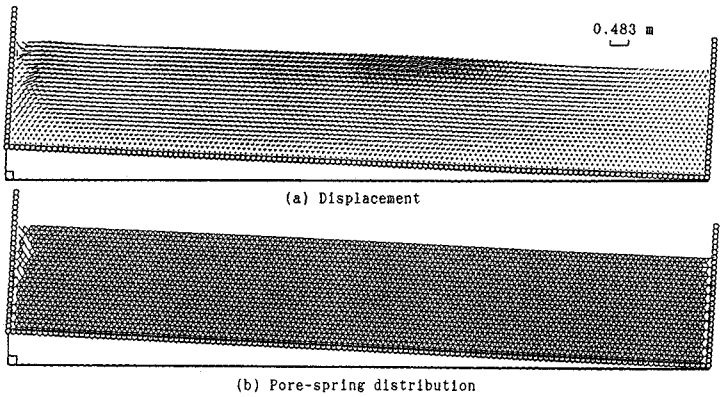

Fig. 12 Pseudo-static analysis with DEM (K_h=0.2).

uniform through layers.

The seismic coefficient is increased to K_h=0.3 in Fig. 11. Fig. 11 (b) shows that the failure zone extends from the A_{sd} layers through the surface layer. The amount of displacement illustrated in Fig. 11 is only a tentative value after a series of iterations where a considerable imbalance still remains between the external force and internal resistance. Judging from Fig. 11, this ground can be determined to have exceeded its limit equilibrium for K_h=0.3. The critical acceleration of this ground can be estimated about

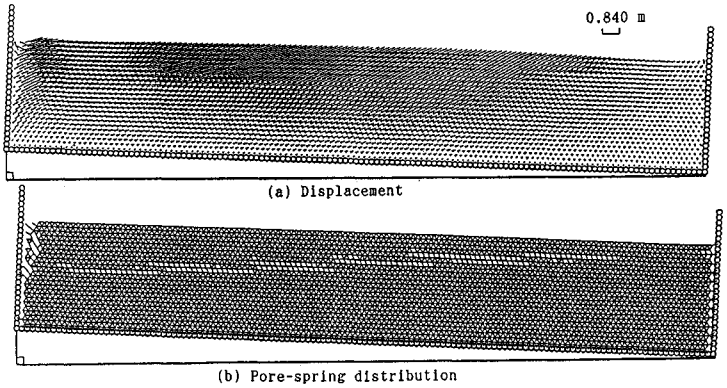

Fig. 13 Pseudo-static analysis with DEM (K_h=0.3)

0.25 g, its failure surface coinciding with A_{sd} layers marked in Fig. 10(b).

(2) Critical acceleration and failure mode of the ground by DEM

Lateral acceleration of 0.2 g and 0.3 g is applied to the DEM model. Figs. 12 and 13 illustrate the distributions of displacements and pore-springs for K_h=0.2, and K_h=0.3, respectively. In Fig. 13(b) pore-springs show a failure surface along the A_{sd} layers. Comparing these results with the FEM computation, the DEM model can be regarded to have simulated critical acceleration and failure mode of the slope almost consistently except near the boundaries.

In the DEM idealization, the elements are confined in a rigid box as depicted in Fig. 8, whereas horizontal rollers are adopted for both sides of the slope in the FEM model. The latter boundary condition implies that the model repeats itself infinitely in the configuration of the actual slope illustrated in Fig. 5, the true boundary condition appears to be in between the two. Fig. 5 also shows that most of the sliding occurs at the middle of the actual slope, where the effect of the boundary condition is small in the long DEM model. Therefore we proceeded to the sliding analysis without modifying the parameters and boundary conditions of the DEM model.

(3) Sliding analysis with the DEM model

The permanent displacement of the ground is calculated by pseudo-static analysis with the DEM model. The effect of liquefaction is incorporated in the DEM model as follows :

① According to Hamada *et al.*, A_{sd} and A_{st} layers are identified to have liquefied (Fig. 5). These are layer #4 and 6 in Table 1 and Fig. 8.

② The pore-springs of these layers are cut off (see Fig. 8(c)).

③ The element-spring constants in both normal and tangential direction of these layers are reduced to 1/10, 1/50, 1/100 of the initial values.

④ Lateral acceleration of 0.1 g (K_h=0.1) is applied during computation.

The first three steps allow free shear deformation of the liquefied layers. The reduction in the normal spring constants cause large volumetric change of the liquefied zone. This is likely to occur in the actual case due to, for example, boiling and dissipation of the pore water into the surrounding soil layers. Usually, the excess pore water pressure builds up and reaches its maximum after the peak acceleration has passed away. Hamada (1986) reports that strange sound was heard that might have indicated ground movement an hour after the earthquake. Hence, we assume that the sliding takes place after the main part of the ground motion goes by. Therefore, seismic coefficient of 0.1 is chosen in this pseudo-static analysis. This value and location of the liquefied layers are parts of the assumptions of this analysis rather than its condition.

Fig. 14 illustrate displacement distributions of Case 1, where the spring constants of the liquefied layers are reduced to 1/10 of the original values. The sliding only occurs on the left hand side of the model. At

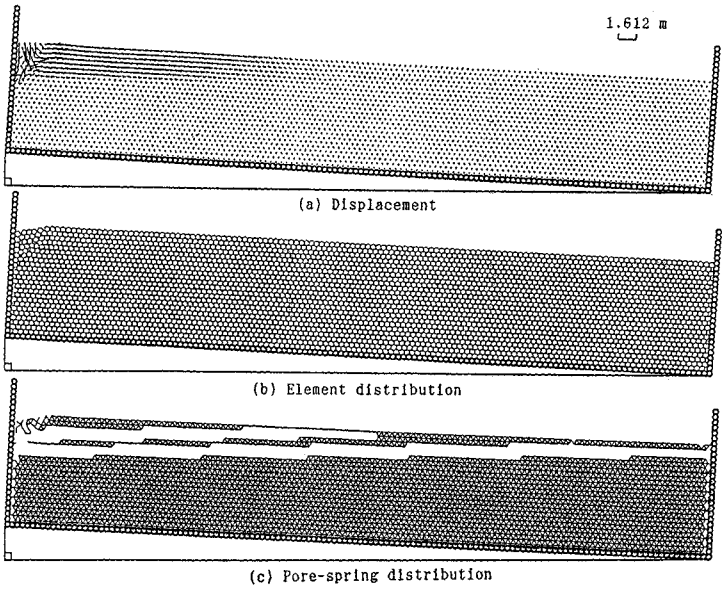

Fig. 14 Result of sliding analysis of Noshiro City with DEM model (Case 1).

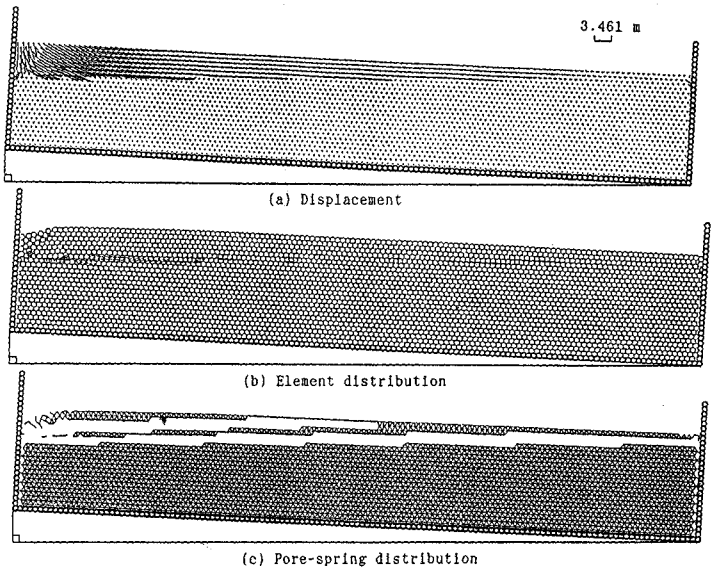

Fig. 15 Result of sliding analysis of Noshiro City with DEM model (Case 2).

this side, the liquefied layer is more than twice as thick as that of the other side.

Figs. 15 and 16 show displacement of Case 2 and Case 3, where the normal element spring constants are reduced to 1/50 and 1/100 of the original values respectively. In Case 3, the sliding appears throughout the surface layers except for those elements near the right side boundary. This case also exhibits a considerable settlement that is conspicuous on the left-hand side. The amount of the settlement is about 10 cm, 50 cm, 100 cm in Case 1, Case 2 and Case 3, respectively. Although its magnitude is unknown, similar settlement could have probably occurred in the actual slope due to the loss of liquefied sand through vertical cracks and dissipation of the pore water.

In Fig. 15 is depicted a mechanism of movement of the slope. Settlement and sliding are combined and propagate through the surface layers starting from the left-hand (up hill) side where the thickness of the

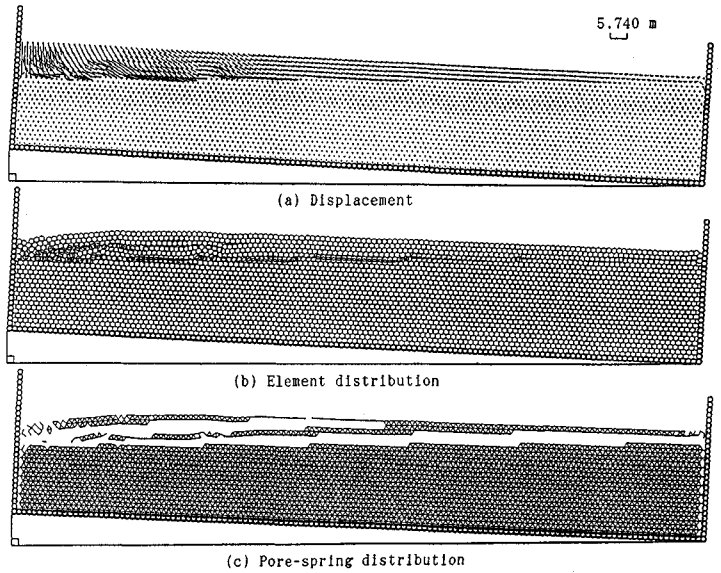

Fig. 16 Result of sliding analysis of Noshiro City with DEM model (Case 3).

liquefied layers is the largest. The more the volumetric change of the liquefied zone is exaggerated, the more dynamic and wide-spread the movement becomes. The actual sliding is reported about 3 meters (Fig. 4). Computed sliding displacements in cases 2 (3.3 m) and 3 (4.9 m) are similar to the observed values.

5. DISCUSSIONS

The mechanism of the ground movement due to subsurface liquefaction has not been clarified. Yet, some simple computations can be informative. Firstly, sliding block on a smooth plane inclined 2.6 degrees from the horizontal will slide down at the rate of $9.8 \sin 2.6^\circ = 0.44$ m/s^2. In 9 seconds, it will slide 3 m and have 4 m/s of velocity. This kind of rapid movement is inconceivable to have occurred in the reported cases. Towhata (1987) showed that similar end displacement can be computed by idealizing the surface layer as a linear truss on a smooth inclined plane with one end free and the other fixed.

Out of 60 field observations, Hamada *et al.* (1986) have obtained a regression equation of the magnitude of the permanent displacement D (m) of the ground against the thickness of the liquefied layer H (m) and the larger gradient of the ground surface or the lower boundary face of the liquefied layer θ (%).

$$D = 0.75 \cdot \sqrt[3]{H} \cdot \sqrt[3]{\theta} \quad \cdots\cdots (18)$$

The two independent valuables of this equation can be interpreted as conditions of the liquefied layer itself. This observation suggests that the phenomenon of permanent displacement due to subsurface liquefaction should be analyzed by considering the liquefied zone not as a plane of zero thickness but as a body. Both its shearing and volumetric deformations are important.

In the DEM analysis, the permanent displacement of a slope in Noshiro city was simulated as combination of settlement and sliding. As is shown in cases 1 through 3 where degree of volumetric change of the liquefied zone is controlled, the magnitude of the movement depends on the magnitude of volumetric change. The volumetric change and succeeding settlement of the surface layer were found to initiate the lateral movements. This seems to apply to many cases where after shear resistance loss of a specific layer the slope can still be stable. For example, the layer has little initial shear stress or the other layers can stand for it by truss effect or arch action.

6. CONCLUSIONS

The permanent displacement of a slope due to subsurface liquefaction was simulated by Distinct Element Model. Out of this study, the following can be concluded :

(1) By using the Distinct Element Model instead of the SDOF system in the sliding block analysis, a new procedure was constructed. This can be applied to soil-structure interaction problems with large deformation where the sliding block model is mechanically too simplistic.

(2) The permanent displacement of a slope in Noshiro City was simulated by Distinct Element Analysis. The movement of the slope was found to be a combination of the settlement and lateral sliding.

(3) Volumetric deformation of the liquefied zone itself was identified as the most influential factor to the permanent displacement.

ACKOWLEDGEMENT

The authors are indebted for valuable suggestions to professors Motohiko Hakuno (University of Tokyo) and Masanori Hamada (Tokai University).

REFERENCES

1) Cundall, P. A. : A Computer Model for Simulating Progressive Large Scale Movement in Blocky Rock System, Symp. ISRM, Nancy, France, Proc. Vol. 2, pp. 129-136, 1971.
2) Hakuno, M. and Tarumi, Y. : A Granular Assembly Simulation for the Seismic Liquefaction of Sand, Structural Eng./Earthquake Eng., Vol. 5, No. 2, pp. 129-138 (Proc. of JSCE No. 398), 1988.
3) Hamada, M., Yasuda, S., Isoyama, R. and Emoto, K. : Measurement and Considerations on the Permanent Ground Displacement due to Liquefaction, Proc. JSCE, Vol. 376/III-6, 1986.
4) Hamada, M., Yasuda, S., Isoyama, R. and Emoto, K. : Study on Liquefaction Induced Permanent Ground Displacements, Association for The Development of Earthquake Prediction, Nov., 1986.
5) Igarashi, S. and Hakuno, M. : The Response of Mass-on-Rough-Plane Model due to Earthquakes, Proc. JSCE, No. 380/I-7, 1987.
6) Ishihara, K. and Towhata, I. : Response Analysis of Soil Layers Considering Liquefaction, Proceedings of the 14th Conference of Geotechnical Engineering in Japan, pp. 1305-1308, 1978.
7) Iwashita, K. and Hakuno, M. : Granular Assembly Simulation for Dynamic Cliff Collapse due to Earthquake, Proc. of 9 WCEE, Vol. 3, pp. 175-180, 1988.
8) Meguro, K. and Hakuno, M. : Fracture Analyses of Concrete Structures by Granular Assembly Simulation, Bulletin of the Earthquake Research Institute, University of Tokyo, Vol. 63, Part 4, pp. 409-468, 1988 (Japanese with English abstract).
9) Meguro, K. and Iwashita, K. and Hakuno, M. : Fracture Tests of Masonry Concrete Elements by Granular Assembly Simulation, Proc. of 9 WCEE (Ninth World Conference on Earthquake Engineering), Vol. 6, pp. 181-186, 1988.
10) Meguro, K. and Hakuno, M. : Fracture Analyses of Concrete Structures by the Modified Distinct Element Method, Structural Eng./Earthquake Eng., Vol. 6, No. 2, pp. 283-294 (Proc. of JSCE No. 410), 1989.
11) Mogami, T. : A Statical Approach to the Mechanics of Granular Materials, Soil and Foundations, Vol. V, No. 2, pp. 26-36, 1965.
12) Newmark, N. M. : Effects of Earthquakes on Dams and Embankments, Geotechnique, Vol. 15, No. 2, pp. 139-160, Jan., 1965.
13) Towhata, I. : Analysis of Slip Displacement Due to Liquefaction, Proc. of 18th Conference on Geotechnical Engineering in Japan, 1987.

(Received November 21 1989)